Robotica (2002) volume 20, pp. 329–339. © 2002 Cambridge University Press
DOI: 10.1017/S0263574701004039 Printed in the United Kingdom

Dynamic modeling of structurally-flexible planar parallel manipulator

Bongsoo Kang and James K. Mills

Department of Mechanical and Industrial Engineering, University of Toronto, 5 King's College Road, Toronto, Ontario (Canada) M5S 3G8
E-mail: kang@mie.utoronto.ca and mills@mie.utoronto.ca

(Received in Final Form: December 10, 2001)

SUMMARY

This paper presents a dynamic model of a planar parallel manipulator including structural flexibility of several linkages. The equations of motion are formulated using the Lagrangian equations of the first type and Lagrangian multipliers are introduced to represent the geometry of multiple closed loop chains. Then, an active damping approach using a PZT actuator is described to attenuate structural vibration of the linkages. Overall dynamic behavior of the manipulator, induced from structural flexibility of the linkage, is well illustrated through simulations. This analysis will be used to develop a prototype parallel manipulator.

KEYWORDS: Planar parallel manipulator; Structural flexibility; Active damping

1. INTRODUCTION

A high speed pick-and-place positioning mechanism is an indispensable element in various industrial fields, especially in electronic manufacturing, where small product size and short assembly times characterize the manufacturing process. The essential functions of these mechanisms are their speed and precision. Current manipulators, carrying out this task, typically consist of multiple linear orthogonal axes. This serial type structure is easy to develop and analyze. However, the inertia of the axis hardware, including actuators, has a very significant influence on the performance of supporting axis.

To overcome inherent disadvantages of serial types structures such as X-Y tables and gantry robots, planar parallel manipulators have been proposed and investigated.[1–3] These devices usually consist of three closed chains with one platform, which corresponds to an end-effector. Depending on which types of joints are used in one chain, these devices are classified as RRR, RPR, PPP, etc. Here, R stands for a revolute joint and P for a prismatic joint. Since the actuators are fixed to the base and three linkages support the moving platform, this structure has high mechanical stiffness and low inertia, which results in high positioning accuracy and rapid motion capability. However, dynamic modeling of a parallel manipulator is more complex than that of a serial type manipulator because there are several closed chains between the actuators and the platform. Previous approaches include the traditional Newton-Euler method,[4] the Lagrangian formulation,[5] and the principle of virtual work.[6, 7] A review of these approaches can be found in Tsai.[8]

Moreover, we must consider structural flexibility of linkages in modeling a parallel manipulator as industry demands high-speed machines, and hence lightweight linkages which deform under high inertial forces. For a serial type manipulator with structural flexibility, results of an unconstrained manipulation have been presented in Book[9] and Low,[10] and results of a constrained manipulation in Hu[11] and Krishnamurthy.[12] If serial types manipulators with structural flexibility cooperate with each other[12, 13] or rigid manipulators work together to handle a flexible payload[14] or follow prescribed trajectories, keeping contact with stiff environment,[11] the system is then configured as a closed loop chain with rigid-flexible combination. This is similar to a parallel manipulator with flexibility. However, a direct dynamic model for a parallel manipulator, including structural flexibility, has been the subject of few studies. Yuan[15] formulated dynamics of a parallelogram mechanism with flexible links by the assumed mode method and Fattah[16] modeled a 3-DOF spatial parallel manipulator with flexible links using the finite element method.

In this paper, the equations of motion for a planar parallel manipulator with structurally flexible linkages are formulated using the Lagrangian equations of the first type. With constraint equations representing the geometry of multiple closed loop chains – typical characteristic of a parallel manipulator, Lagrangian multipliers are introduced to avoid complexity in calculating passive coordinates of the parallel manipulator. Then, an active damping approach using a piezoelectric material, lead zirconium titanate (PZT), is described to attenuate structural vibration of linkages. Attaching to the surface of the linkages, the PZT actuator produces a bending moment according to a linear velocity (L-type) feedback control scheme[17] so that vibration of the linkage can be damped. Simulations are performed to verify the proposed equations of motion and investigate feasibility of active structural vibration damping using PZT actuators.

The paper is organized as follows. Section 2 describes the architecture of a parallel manipulator and its dynamic modeling. Section 3 gives an active damping method for vibration of linkages and Section 4 gives simulation results. Finally, conclusions are given in Section 5.

https://doi.org/10.1017/S0263574701004039 Published online by Cambridge University Press

2. DYNAMIC MODELING

2.1. Architecture

The architecture of the parallel mechanism considered is illustrated in Figure 1. The platform has a regular triangular shape and is supported by three intermediate links assumed to exhibit structural flexibility. Therefore, vibration of the linkage gives a direct influence on motions of the platform. Both ends of the intermediate link are composed of non-actuated revolute joints. A slider connecting with the linkage is driven by a linear actuator. The proposed planar manipulator is categorized as a PRR type, because one closed chain consists of the prismatic joint and two consecutive revolute joints. In contrast to well-known RPR type parallel manipulators, the actuator hardware of the proposed PRR configuration remains stationary, resulting in low inertia of moving parts. With appropriately selected kinematic parameters, listed in Table I, the reachable workspace of the manipulator is approximately 400 mm * 400 mm.

Generalized coordinates for dynamic formulation of the manipulator are shown in Figure 2. The position and orientation of the platform at its mass center is written with respect to the fixed X-Y coordinate system as

$$\bar{X}_P = [x_P \;\; y_P \;\; \varphi]^T \tag{1}$$

The origin of the fixed coordinate system is located on the point where imaginary extended lines of three actuators intersect. The distances of sliders from A_i, which correspond to solutions to an inverse kinematic problem, are expressed as

$$\bar{\rho} = [\rho_1 \;\; \rho_2 \;\; \rho_3]^T \tag{2}$$

Three linkages including associated coordinates are numbered with a subscript starting from the right linkage, in a counterclockwise direction. β_i is defined as the angle between the X-axis of the fixed frame and the i^{th} intermediate link and α_i is the constant angle between the X-axis of the fixed coordinate frame and the i^{th} linear actuator.

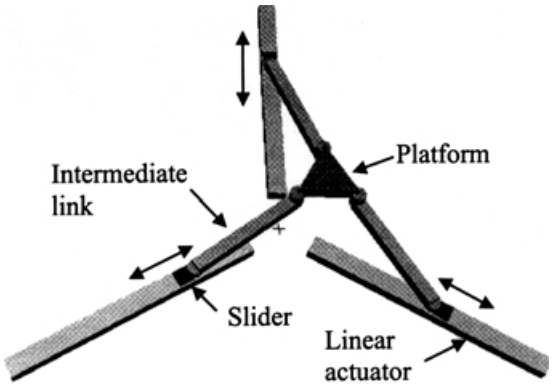

Fig. 1. Configuration of the parallel manipulator.

Table I. Kinematic parameters.

Platform (side length)	100 mm
Intermediate link	200 mm
Linear actuator	400 mm
Angle of linear actuator (α)	120,270,30 (degree)

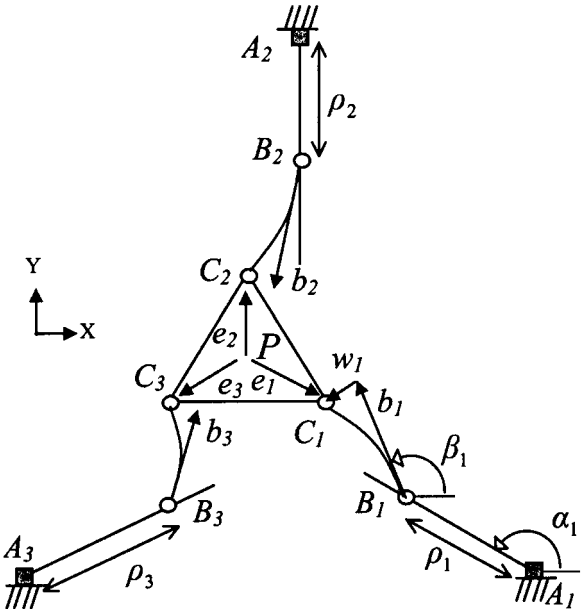

Fig. 2. Coordinate system of parallel manipulator.

From the geometry of Figure 2, coordinates of point C_i are written as

$$x_{ci} = x_{ai} + \rho_i \cos\alpha_i + l\cos\beta_i - w_i(l)\sin\beta_i \tag{3}$$

$$y_{ci} = y_{ai} + \rho_i \sin\alpha_i + l\sin\beta_i + w_i(l)\cos\beta_i \tag{4}$$

where x_{ai} and y_{ai} are coordinates of point A_i and l is length of the linkage. $w_i(l)$ is defined as a lateral deformation at the end of the linkage, C_i, due to flexibility of the linkage. Since length of the linkage is long compared with the thickness of the linkage, the linkage can be treated as an Euler-Bernoulli beam. The coordinates of point C_i can be formulated using the platform coordinates as

$$x_{ci} = x_p + x'_{ci}\cos\varphi - y'_{ci}\sin\varphi \tag{5}$$

$$y_{ci} = y_p + x'_{ci}\sin\varphi + y'_{ci}\cos\varphi \tag{6}$$

x'_{ci} and y'_{ci} are constant coordinates measured from mass center of the platform when φ is zero. From equations (3–6), a closed-form solution is calculated as

$$\rho_i = M_i \pm \sqrt{l^2 + w_i^2 - S_i^2} \qquad i = 1, 2, 3 \tag{7}$$

where:

$$M_i = (x_{ci} - x_{ai})\cos\alpha_i + (y_{ci} - y_{ai})\sin\alpha_i$$

$$S_i = (x_{ci} - x_{ai})\sin\alpha_i - (y_{ci} - y_{ai})\cos\alpha_i$$

Since there are two possible solutions for each chain, this manipulator can take on a maximum of eight configurations for a set of given coordinates of the platform. Additionally, large linkage deformation may lead to no solution because the right-hand side of equation (7) has a negative value.

2.2. Dynamic analysis

Evaluation of the derivative of equations (3)–(6) with respect to time, gives

$$(\dot{x}_P\bar{i} + \dot{y}_P\bar{j}) + \dot{\varphi}(\bar{k}\times\bar{e}_i) = \dot{\rho}_i\bar{a}_i + (\dot{\beta}_i + \dot{w}_i(l)/l)(\bar{k}\times\bar{b}_i) \tag{8}$$

https://doi.org/10.1017/S0263574701004039 Published online by Cambridge University Press

where:

$$\bar{a}_i = \cos(\alpha_i)\bar{i} + \sin(\alpha_i)\bar{j}$$

$\dot{x}_P$, $\dot{y}_P$, $\dot{\varphi}$ are a linear velocity and an angular velocity of the platform respectively. Dot-multiplication of equation (8) by $\bar{b}_i$ leads to

$$\dot{\rho}_i = \frac{1}{\bar{a}_i \cdot \bar{b}_i} [b_{ix} \;\; b_{iy} \;\; e_{ix}b_{iy} - e_{iy}b_{ix}][\dot{x}_P \;\; \dot{y}_P \;\; \dot{\varphi}]^T = J_{Pi}\dot{\bar{X}}_P \qquad (9)$$

where:

$$\bar{b}_i = b_{ix}\bar{i} + b_{iy}\bar{j} \text{ and } \bar{e}_i = e_{ix}\bar{i} + e_{iy}\bar{j}$$

Cross-multiplication of equation (8) by $\bar{b}_i$ gives

$$\dot{\beta}_i = \frac{1}{l^2}\{[-b_{iy} \;\; b_{ix} \;\; e_{ix}b_{ix} + e_{iy}b_{iy}] - (\bar{b}_i \times \bar{a}_i) J_{Pi}\}\dot{\bar{X}}_P - \dot{w}_i(l)/l \qquad (10)$$

Acceleration of the moving part can be formulated through a similar procedure as follows;

$$\ddot{\rho}_i = \frac{1}{\bar{a}_i \cdot \bar{b}_i}\{[b_{ix} \;\; b_{iy} \;\; e_{ix}b_{iy} - e_{iy}b_{ix}]\ddot{\bar{X}}_P - \bar{b}_i \cdot \bar{e}_i \dot{\varphi}^2 + \dot{\beta}_i^2 l^2 + \dot{\beta}_i \dot{w}_i(l) l\} \qquad (11)$$

$$\ddot{\beta}_i = \frac{1}{l^2}\{[-b_{iy} \;\; b_{ix} \;\; e_{ix}b_{ix} + e_{iy}b_{iy}]\ddot{\bar{X}}_P - (\bar{b}_i \times \bar{e}_i)\dot{\varphi}^2 - (\bar{b}_i \times \bar{a}_i)\ddot{\rho}_i\} - \ddot{w}_i(l)/l \qquad (12)$$

Flexible deformations can be expressed by the product of time-dependant functions and position-dependant functions, i.e. an assumed modes model;

$$w_i(x, t) = \sum_{j=1}^{r} \eta(t)_{ij}\psi_j(\xi) \qquad i = 1, 2, 3 \qquad (13)$$

where $\xi = x/l$. r is the number of assumed modes. Considering boundary conditions of the linkage on B_i and C_i, normalized shape functions satisfying a pin-free boundary condition are selected as

$$\psi_j(\xi) = \frac{1}{2\sin(\gamma_j)}\left[\sin(\gamma_j\xi) + \frac{\sin(\gamma_j)}{\sinh(\gamma_j)}\sinh(\gamma_j\xi)\right] \qquad (14)$$

where:

$$0 \le \xi \le 1 \text{ and } \gamma_j = (j + 0.25)\pi \qquad j = 1, 2, \ldots, r$$

Figure 3 shows shape functions within the first four modes. Integrating all generalized coordinates into a single vector X as

$$X = [\bar{\rho} \;\; \bar{\beta} \;\; \bar{X}_P \;\; \bar{\eta}]^T \in R^{9+3r} \qquad (15)$$

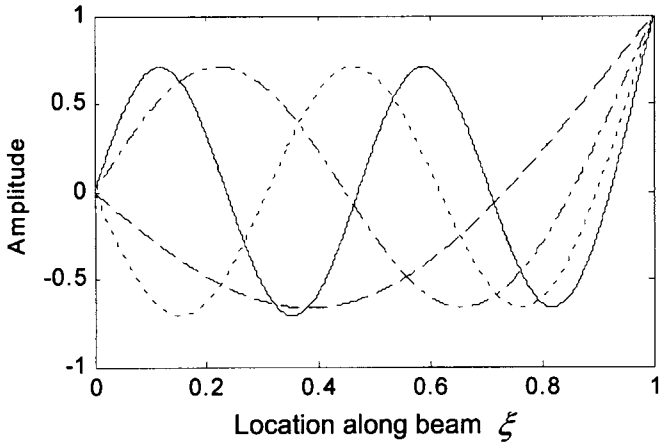

Fig. 3. Amplitude of first four mode shapes of straight beam vs. location along beam ξ
(dashed line: first mode; dash-dot line: second mode; dotted line: third mode; solid line: fourth mode).

where:

$$\bar{\beta} = [\beta_1 \;\; \beta_2 \;\; \beta_3]^T$$

$$\bar{\eta} = [\eta_{11} \;\; \cdots \;\; \eta_{1r} \;\; \eta_{21} \;\; \cdots \;\; \eta_{2r} \;\; \eta_{31} \;\; \cdots \;\; \eta_{3r}]^T$$

Using inertia parameters of the manipulator and generalized coordinates, the kinetic energy is written as

$$T = \sum_{i=1}^{3}\frac{1}{2}m_s\dot{\rho}_i^2 + \frac{1}{2}m_P(\dot{x}_P^2 + \dot{y}_P^2) + \frac{1}{2}I_P\dot{\varphi}^2 + \sum_{i=1}^{3}\frac{1}{2}\int \rho_A[\dot{\rho}_i^2 + (x\dot{\beta}_i + \dot{w}_i)^2 + 2\dot{\rho}_i(x\dot{\beta}_i + \dot{\omega}_i)\sin(\alpha_i - \beta_i)]\,dx \qquad (16)$$

and potential energy due to deformation of the linkage is given as

$$V = \sum_{i=1}^{3}\int EI(w_i'')^2\,dx \qquad (17)$$

where m_s is mass of the slider, and m_p, I_p are mass and mass moment of inertia of the platform respectively. ρ_A, E, I are mass per length, elastic modulus, and area moment of inertia of the linkage. Evaluating Lagrangian equations of the first type given by

$$\frac{d}{dt}\left(\frac{\partial T}{\partial \dot{X}_i}\right) - \frac{\partial(T - V)}{\partial X_i} = Q_i + \sum_{k=1}^{m}\lambda_k\frac{\partial \Gamma_k}{\partial X_i} \qquad (18)$$

where Q_i is generalized force. λ_k and Γ_k are the k^{th} Lagrangian multiplier and constraint equation respectively,

https://doi.org/10.1017/S0263574701004039 Published online by Cambridge University Press

the left-hand side of equation of motions is formulated as follows:

$$\frac{d}{dt}\left(\frac{\partial T}{\partial \dot{\rho}_i}\right)-\frac{\partial (T-V)}{\partial \rho_i}$$

$$=(m_s+m)\ddot{\rho}_i+0.5ml\,\sin(\alpha_i-\beta_i)\ddot{\beta}_i$$

$$+\sum_{j=1}^{r}\ddot{\eta}_{ij}\sin(\alpha_j-\beta_i)\int\rho_A\psi_j\,dx-0.5ml\cos(\alpha_i-\beta_i)\dot{\beta}_i^2$$

$$-\sum_{j=1}^{r}\dot{\eta}_{ij}\dot{\beta}_i\cos(\alpha_i-\beta_i)\int\rho_A\psi_j\,dx \qquad i=1,2,3 \quad (19)$$

$$\frac{d}{dt}\left(\frac{\partial T}{\partial \dot{\beta}_i}\right)-\frac{\partial (T-V)}{\partial \beta_i}$$

$$=0.5ml\,\sin(\alpha_i-\beta_i)\ddot{\rho}_i+ml^2\ddot{\beta}_i/3+\sum_{j=1}^{r}\ddot{\eta}_{ij}\int\rho_A x\psi_j\,dx$$

$$+\sum_{j=1}^{r}\dot{\eta}_{ij}\dot{\rho}_i\cos(\alpha_i-\beta_i)\int\rho_A\psi_j\,dx \qquad i=1,2,3 \quad (20)$$

$$\frac{d}{dt}\left(\frac{\partial T}{\partial \dot{X}_P}\right)-\frac{\partial (T-V)}{\partial X_P}=\begin{bmatrix} m_P & 0 & 0\\ 0 & m_P & 0\\ 0 & 0 & I_P\end{bmatrix}\begin{bmatrix}\ddot{x}_P\\ \ddot{y}_P\\ \ddot{\varphi}\end{bmatrix} \quad (21)$$

$$\frac{d}{dt}\left(\frac{\partial T}{\partial \dot{\eta}_{ij}}\right)-\frac{\partial (T-V)}{\partial \eta_{ij}}$$

$$=\sin(\alpha_i-\beta_i)\ddot{\rho}_i\int\rho_A\psi_j\,dx+\ddot{\beta}_i\int\rho_A x\psi_j\,dx+\ddot{\eta}_{ij}\int\rho_A\psi_j^2\,dx$$

$$-\int\rho_A\psi_j\,dx\cos(\alpha_i-\beta_i)\dot{\beta}_i\dot{\rho}_i+\int EI(\psi_j'')^2\,dx$$

$$i=1,2,3 \text{ and } j=1,2,\ldots,r \quad (22)$$

From the geometry of three closed loop chains, equations (3)–(6), six constraint equations are given by

$$\Gamma_{2i-1}=\rho_i\cos\alpha_i+l\cos\beta_i-\sum_{j=1}^{r}\eta_{ij}\sin\beta_i-x_P-r\cos(\varphi_i+\varphi) \quad (23)$$

$$\Gamma_{2i}=\rho_i\sin\alpha_i+l\sin\beta_i+\sum_{i=1}^{r}\eta_{ij}\cos\beta_i-y_P-r\sin(\varphi_i+\varphi) \quad (24)$$

where:

$$r\cos(\varphi_i)=x'_{ci},\ r\sin(\varphi_i)=y'_{ci} \qquad i=1,2,3$$

Through equations (23) and (24), the right-hand side of equation (18) is

$$F_i+\sum_{k=1}^{6}\lambda_k\frac{\partial \Gamma_k}{\partial \rho_i}=F_i+\lambda_{2i-1}\cos\alpha_i+\lambda_{2i}\sin\alpha_i$$

$$i=1,2,3 \quad (25)$$

where F_i is output of the i^{th} linear actuator.

$$\sum_{k=1}^{6}\lambda_k\frac{\partial \Gamma_k}{\partial \beta_i}=\lambda_{2i-1}\left(-l\sin\beta_i-\sum_{j=1}^{r}\eta_{ij}\cos\beta_i\right)$$

$$+\lambda_{2i}\left(l\cos\beta_i-\sum_{j=1}^{r}\eta_{ij}\sin\beta_i\right) \qquad i=1,2,3 \quad (26)$$

$$F_{ext}+\sum_{k=1}^{6}\lambda_k\frac{\partial \Gamma_k}{\partial X_P}=$$

$$\begin{bmatrix}f_x\\ f_y\\ \tau\end{bmatrix}+\begin{bmatrix}-1 & 0 & -1 & 0 & -1 & 0\\ 0 & -1 & 0 & -1 & 0 & -1\\ s3_1 & c3_i & s3_2 & c3_2 & s3_3 & c3_3\end{bmatrix} \quad (27)$$

where:

$$s3_i=r\sin(\varphi_i+\varphi)\ c3_i=r\cos(\varphi_i+\varphi)$$

F_{ext}, $[f_x\ f_y\ \tau]^T$, is an external force, such as payload, exerted on the platform.

$$\sum_{k=1}^{6}\lambda_k\frac{\partial \Gamma_k}{\partial \eta_{1j}}=-\lambda_1\sin\beta_1+\lambda_2\cos\beta_1 \qquad j=1,2,\ldots,r \quad (28)$$

$$\sum_{k=1}^{6}\lambda_k\frac{\partial \Gamma_k}{\partial \eta_{2j}}=-\lambda_3\sin\beta_2+\lambda_4\cos\beta_2 \qquad j=1,2,\ldots,r \quad (29)$$

$$\sum_{k=1}^{6}\lambda_k\frac{\partial \Gamma_k}{\partial \eta_{3j}}=-\lambda_5\sin\beta_3+\lambda_6\cos\beta_3 \qquad j=1,2,\ldots,r \quad (30)$$

Putting equations (19)–(22) and equations (25)–(30) together, the equations of motion for the planar parallel manipulator are complete with a total of $9+3\times r$ equations;

https://doi.org/10.1017/S0263574701004039 Published online by Cambridge University Press

$$\begin{bmatrix} M_{11} & M_{12} & 0 & M_{14} \\ M_{12}^T & M_{22} & 0 & M_{24} \\ 0 & 0 & M_{33} & 0 \\ M_{14}^T & M_{24}^T & 0 & M_{44} \end{bmatrix} \begin{bmatrix} \ddot{\bar{\rho}} \\ \ddot{\bar{\beta}} \\ \ddot{\bar{X}}_P \\ \ddot{\bar{\eta}} \end{bmatrix} + \begin{bmatrix} V_1 \\ V_2 \\ 0 \\ V_4 \end{bmatrix} + \begin{bmatrix} 0 & 0 & 0 & 0 \\ 0 & 0 & 0 & 0 \\ 0 & 0 & 0 & 0 \\ 0 & 0 & 0 & K \end{bmatrix} \begin{bmatrix} \bar{\rho} \\ \bar{\beta} \\ \bar{X}_P \\ \bar{\eta} \end{bmatrix}$$

$$= \begin{bmatrix} F \\ 0 \\ F_{ext} \\ 0 \end{bmatrix} + \begin{bmatrix} J_{I1} \\ J_{I2} \\ J_{I3} \\ J_{I4} \end{bmatrix} \begin{bmatrix} \lambda_1 \\ \lambda_2 \\ \lambda_3 \\ \lambda_4 \\ \lambda_5 \\ \lambda_6 \end{bmatrix}$$

Each component is expressed in the Appendix.

3. VIBRATION CONTROL

If the intermediate link is very stiff, an appropriate rigid body control method for three linear actuators can yield good tracking performance of the platform.[7] However, structural flexibility of the linkages transfers unwanted vibration to the platform, and may even lead to instability of the system. Since it's hard for three linear actuators to achieve trajectory tracking of the platform and vibration attenuation of linkages simultaneously, an active damping approach is proposed through the use of smart material such as PZT. Attached on the surface of the linkage, the PZT produces a shear force along length of the linkage, which can counteract structural vibration of the linkage. Therefore, the PZT actuators play a role to damp structural vibration of the linkages and three linear actuators produce desired motions of the platform.

A simple proportional and derivative (PD) feedback controller is used for three linear actuators and is given as

$$u_i(t) = -k_P(\rho_{di} - \rho_i) - k_d(\dot{\rho}_{di} - \dot{\rho}_i) \qquad i = 1, 2, 3 \qquad (31)$$

where k_p and k_d are a proportional and a derivative feedback gain respectively. ρ_{di} and $\dot{\rho}_{di}$ are desired values of the i^{th} slider calculated from equations (7) and (9). A linear velocity (L-type) feedback controller is applied to the PZT actuators as

$$V_i(t) = -k_I[\dot{w}_i(a_2, t) - \dot{w}_i(a_1, t)] \qquad i = 1, 2, 3 \qquad (32)$$

where k_I is a linear velocity feedback gain for PZT. a_1 and a_2 denotes positions of both ends of the PZT actuator measured from B_i along the linkage. Assuming a perfectly bonded static model,[18] the virtual work-done by the i^{th} PZT actuator is evaluated as

$$\delta W_{PZT} = cV_i(t) \sum_{j=1}^{r} [\psi_j'(a_2) - \psi_f'(a_1)]\delta\eta_{ij} \qquad (33)$$

where c is a positive constant expressing the bending moment applied voltage.

The stability of the L-type control scheme has been addressed by Sun et al.[17] In order to achieve stable control performance, PZT's should be placed in a region on the linkage where $\psi_j(x)$ and $\psi_j'(x)$ have the same trend of variation within $x \in [a_1, a_2]$;

$$(\psi_j(a_2) - \psi_j(a_1))(\psi_j'(a_2) - \psi_j'(a_1)) \geq 0, \qquad (34)$$

Table II. Dynamnic parameters.

Slider	Mass (kg)	0.2
Platform	Mass (kg)	0.2
Intermediate Link	Density (kg/m^3)	2770
	Young's Modulus (GPa)	73
	Dimension (mm)	200 * 25 * 1.5
PZT actuator	Young's Modulus (GPa)	69
	Dimension (mm)	50 * 25 * 0.75
	d_{31} (m/V)	179×10^{-12}

while being positioned away from area of zero strain. Application of this approach to modes of higher frequency is restricted because satisfaction of equation (34) is only achieved in small regions on the linkage, for high frequencies. For the simulation results shown here, a PZT material, QP20N, manufactured by ACX Inc., is selected as a PZT actuator, with its specifications listed in Table II. The placement position of the PZT actuators is adjusted so that the first two vibration modes can satisfy equation (34).

4. SIMULATION RESULTS

Simulations are performed to investigate the flexible behavior of the parallel manipulator utilizing the proposed equations of motion. Dynamic parameters are listed in Table II. The first three modes are considered in the dynamic model, i.e. $r = 3$. A sinusoidal function with smooth acceleration and deceleration is chosen as the desired trajectory;

$$x_P = \frac{x_f}{t_f} t - \frac{x_f}{2\pi} \sin\left(\frac{2\pi}{t_f} t\right) \qquad (35)$$

Considering the target-performance in an electrical assembly process, such as wire bonding in integrated circuit fabrication, the goal for the platform is to move linearly 2 *mm* (x_f) within 10 *msec* (t_f). The trajectory is defined in the direction of the X-axis and feedback gains are listed in Table III. A fourth order Runge-Kutta method was used to integrate the ordinary differential equations at the integration interval of 1 *msec*, using MATLAB™ software.

Figure 4 shows tracking error profiles of the platform when stiffness of the linkages is changed. A rigid-body model, which ignores structural flexibility of the linkages, shows typical characteristics of an underdamped system entering steady state after 30 msec with tracking error decreasing continuously. However, the proposed model with structural flexibility shows persistent oscillation of the platform due to vibration of the linkages. Simulation results with an imaginary material, of which stiffness is ten times larger than a conventional aluminum alloy, while having the same density of the aluminum alloy, are included for

Table III. Feedback control gains.

k_p	10,000 (N/m)
k_d	500 (N-sec/m)
k_I	1,500 (Volts-sec/m)

https://doi.org/10.1017/S0263574701004039 Published online by Cambridge University Press

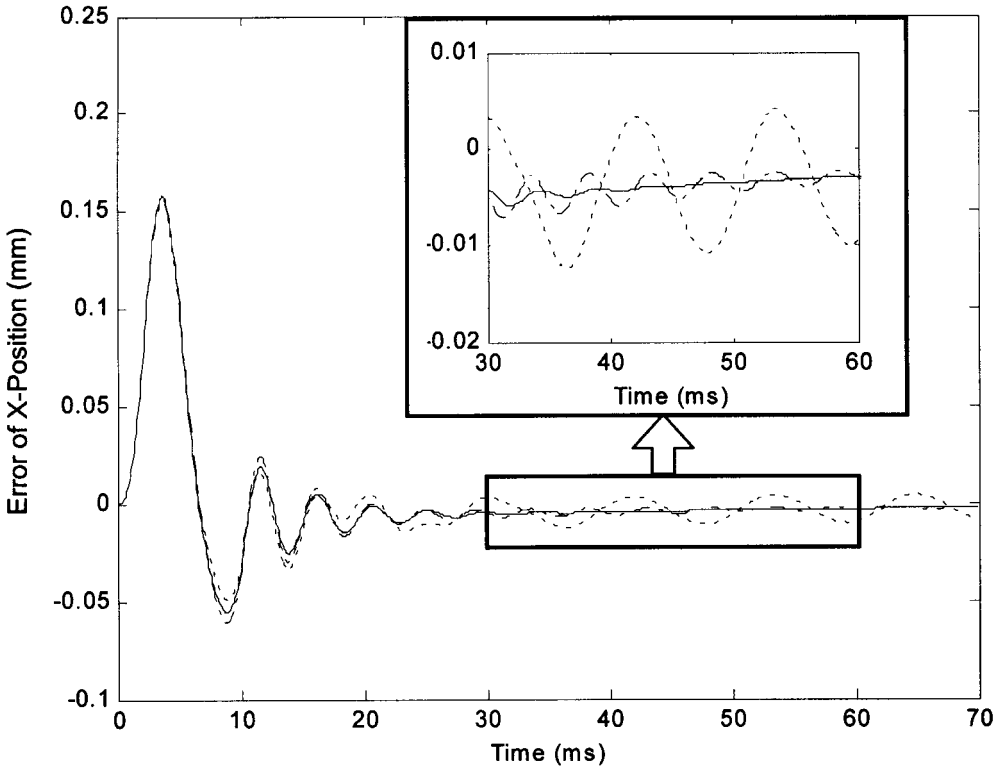

Fig. 4. Error profile of platform for different stiffness of linkage
(solid line: rigid-body model; dotted line: aluminum alloy (Young's Modulus: 73GPa); dash-dot line: ten times stiffer than aluminum alloy (Young's Modulus: 730GPa)).

comparison. The behavior of this system is closer to that of rigid-body model, as shown in Figure 4. The rigid-body model can be thought of a material with infinite stiffness. This comparison is compatible with what is expected intuitively.

Figure 5 shows tracking error profiles with the proposed active damping approach applied to the PZT actuator. In Figures 5–7, 'active damping' means that the PZT actuators are activated to damp vibration of the linkage. 'No damping' means that the PZT actuator is not activated. When the PZT actuators are activated, the tracking error of the platform does not exhibit any vibration in steady state, and the behavior of the platform is similar to that of the rigid-body model, shown in Figure 4. Figure 6 and Figure 7

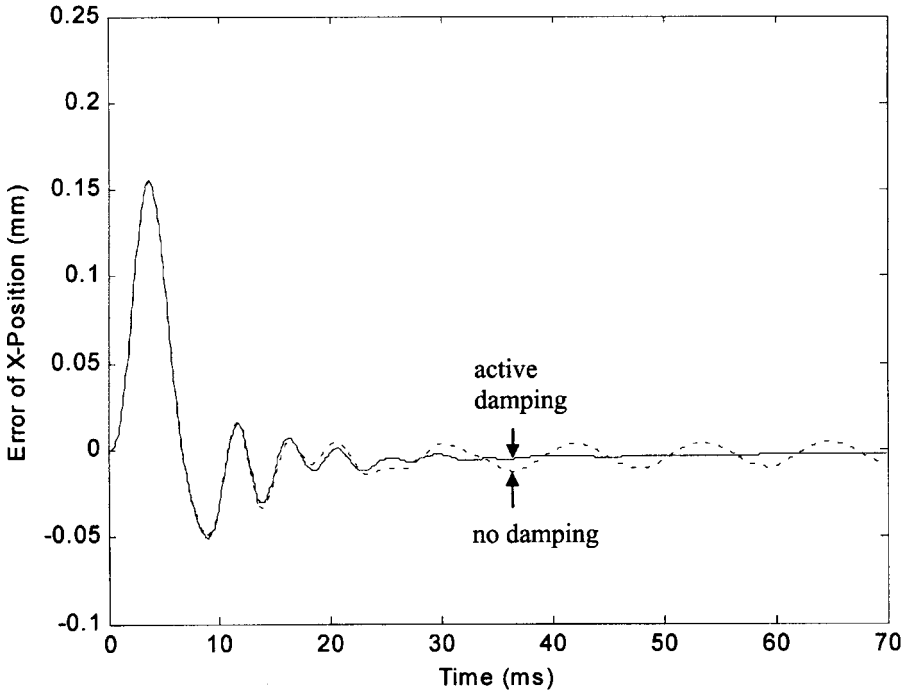

Fig. 5. Error profile of X-directional movement.

https://doi.org/10.1017/S0263574701004039 Published online by Cambridge University Press

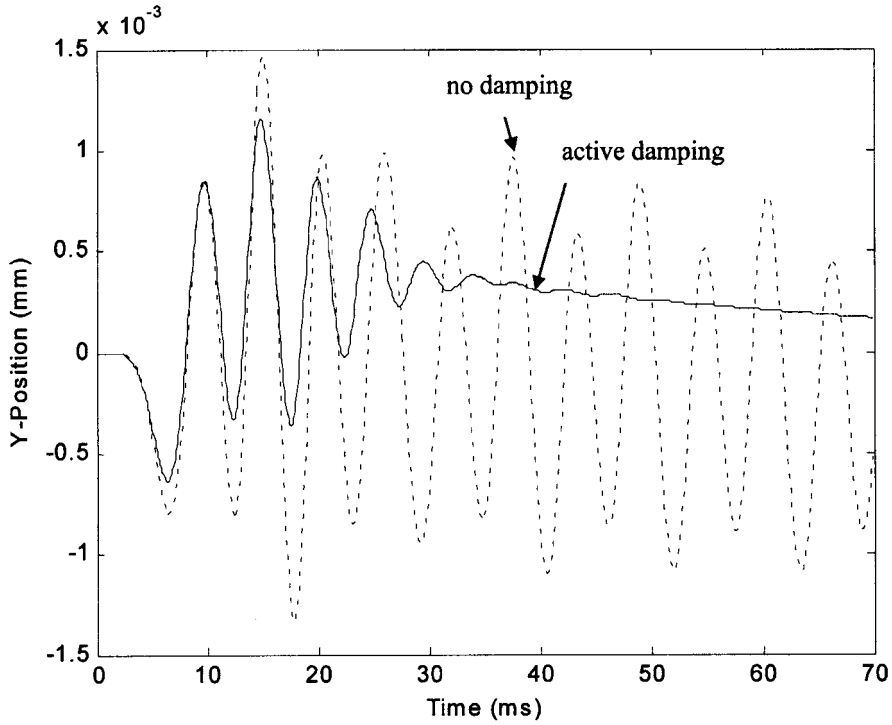

Fig. 6. Y-directional movement.

show the Y-directional movement and the orientation of the platform respectively. These coordinates, which are to maintain the Y-position at 0 meters and orientation at 10 degrees respectively, exhibit oscillations which have been damped out by the active damping approach. In contrast, persistent oscillation is seen without the action of the PZT actuators.

With Figure 8 showing deformation of the linkage on C_i, it reveals that the PZT actuator can damp structural vibration of the linkage effectively. Structural vibrations of the linkages are completely damped after 40 *msec*. The first three vibration modes are illustrated in Figure 9. The first mode has ten times the amplitude than the other modes. The amplitude of the third mode is similar to that of the second mode, because the third mode does not satisfy equation (34), as discussed in last section. However, this does has little or no effect on damping performance, as shown in Figure 8, since the first two modes play a dominant role in vibration. The control output for the first linear actuator is given in the upper plot of Figure 10, and

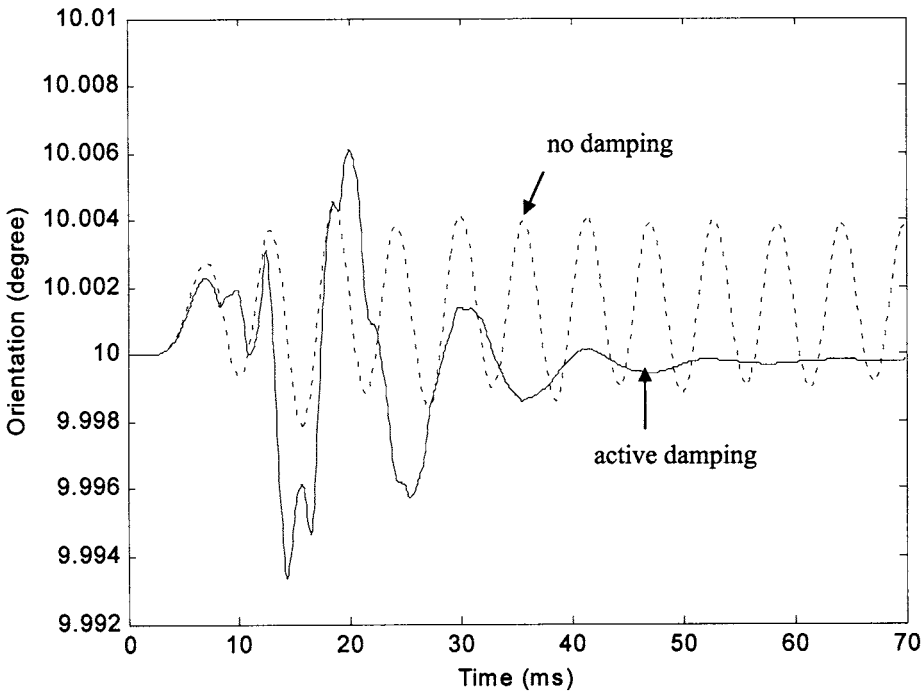

Fig. 7. Orientation of the platform.

https://doi.org/10.1017/S0263574701004039 Published online by Cambridge University Press

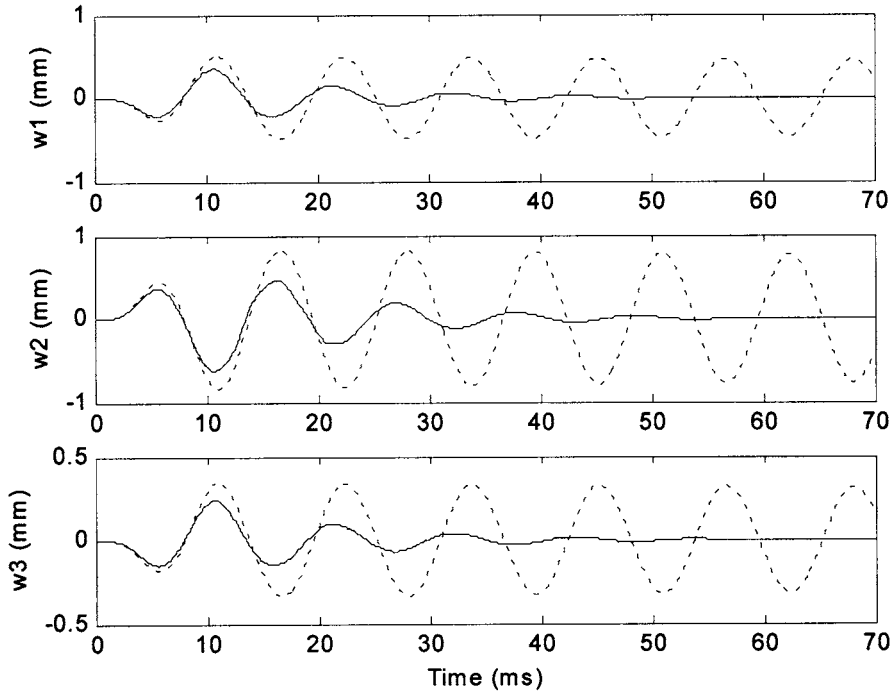

Fig. 8. Flexible deformation of each linkage
(dotted line: no damping; solid line: active damping).

control voltage for the first PZT actuator is shown in the lower plot of Figure 10. Since moving components of the manipulator have small mass moment of inertia, the actuating force is correspondingly small.

5. CONCLUSIONS

The equations of motion for the planar parallel manipulator are formulated by applying the Lagrangian equation of the first type. Introducing Lagrangian multipliers simplifies the complexities that arise due to multiple closed loop chains of the parallel manipulator and the structurally flexible linkages. An active damping method using the PZT actuators is proposed to attenuate structural vibration of the linkage.

Overall dynamic behavior of the parallel manipulator, which cannot be predicted accurately using a rigid-body model, is investigated through the equations of motion. Simulation results show that the parallel manipulator, with lightweight intermediate links, undergoes persistent vibration during fast motion. Additionally, the PZT actuator

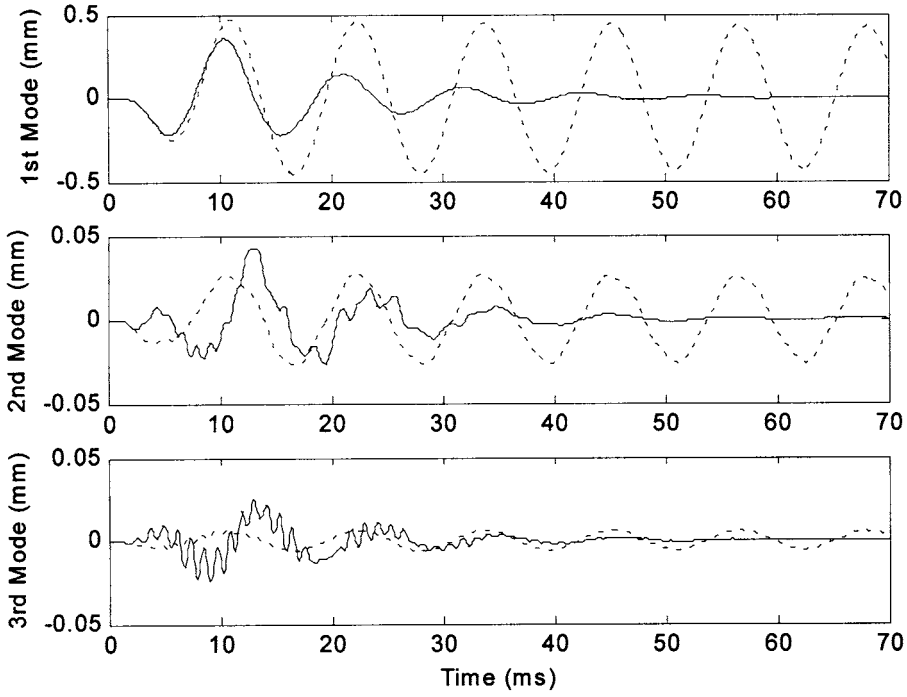

Fig. 9. The first three vibration modes of the first linkage
(dotted line: no damping; solid line: active damping).

https://doi.org/10.1017/S0263574701004039 Published online by Cambridge University Press

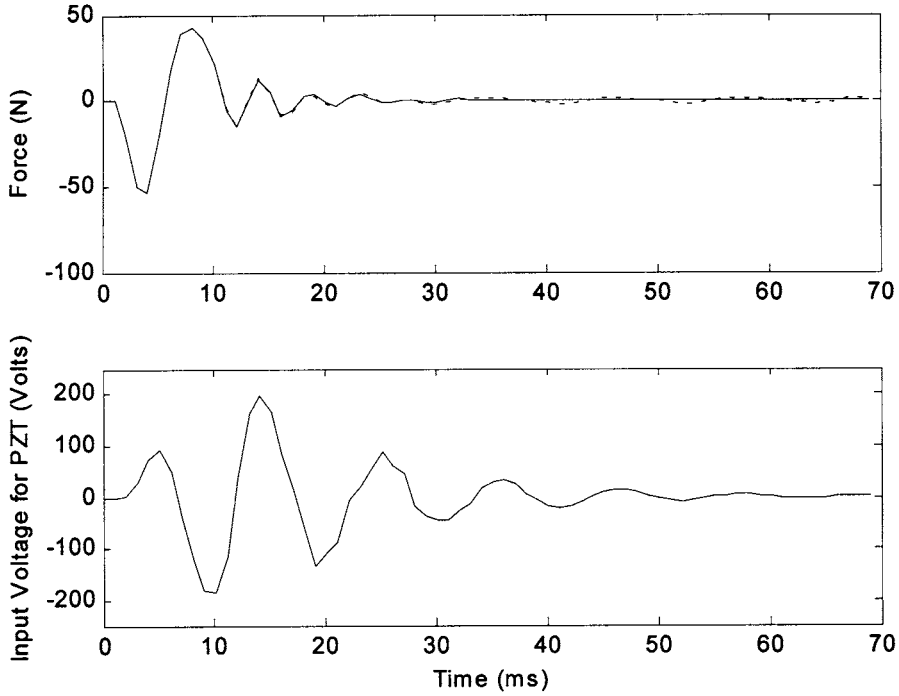

Fig. 10. Control outputs for the 1st actuator
(dotted line: no damping; solid line: active damping).

can provide good damping performance to counteract structural vibration of the linkage, resulting in precise manipulations of the platform. In the near future, we will develop a prototype parallel manipulator based on the presented dynamic analysis.

References

1. C. Gosselin and J. Angeles, "The optimum kinematic design of a planner three-degree-of-freedom parallel manipulator," *ASME Journal of Mechanisms, Transmissions, and Automation in Design* **110**(1), 35–41 (1988).
2. C.M. Gosselin, S. Lemieux and J.-P. Merlet, "A new architecture of planar three-degree of freedom parallel manipulator," *Proc. IEEE International Conference on Robotics and Automation*, Minneapolis, Minnesota (1996) pp. 3738–3743.
3. I.A. Bonev and C.M. Gosselin, "Singularity loci of planar parallel manipulators with revolute joints," *Proc. 2nd Workshop on Computational Kinematics (CK2001)*, Seoul, South Korea (May 20–22, 2001) pp. 291–299.
4. W.Q.D. Do and D.C.H. Yang, "Inverse dynamic analysis and simulation of a platform type of robot," *J. Robotic Systems* **5**(3), 209–227 (1988).
5. H. Pang and M. Shahinpoor, "Inverse dynamics of a parallel manipulator," *J. Robotic Systems* **11**(8), 693–702 (1994).
6. C.D. Zhang and S.M. Song, "An effective method for inverse dynamics of manipulators based on the virtual work principle," *J. Robotic Systems* **10**(5), 605–627 (1993).
7. B. Kang, J. Chu and J.K. Mills, "Design of high speed planar parallel manipulator and multiple simultaneous specification control," *Proc. IEEE International Conference on Robotics and Automation*, Seoul, South Korea (2001) pp. 2723–2728.
8. L.-W. Tsai, *Robot Analysis – The Mechanics of Serial and Parallel Manipulators* (J. Wiley, 1999).
9. W.J. Book, "Recursive Lagrangian dynamics of flexible manipulator arms," *Int. J. Robotics Research* **3**(3), 87–101 (1984).
10. K.H. Low and M. Vidyasagar, "A Lagrangian formulation of the dynamic model for flexible manipulator systems," *ASME J. of Dynamic Systems, Measurement, and Control* **110**, 175–181 (1988).
11. F.L. Hu and A.G. Ulsoy, "Dynamic modeling of constrained flexible robot arms for controller design," *ASME J. of Dynamic Systems, Measurement, and Control* **116**, 56–65 (1994).
12. K. Krishnamurthy and L. Yang, "Dynamic modeling and simulation of two cooperating structurally-flexible robotic manipulators," *Robotica* **13** Part 4, 375–384 (1995).
13. C.J. Damaren, "On the dynamics and control of flexible multibody systems with closed loops," *Int. J. Robotics Research* **19**(3), 238–253 (2000).
14. D. Sun, J.K. Mills and Y. Liu, "Position control of robot manipulators manipulating a flexible payload," *Int. J. Robotics Research* **18**(3), 319–332 (1999).
15. B.-S. Yuan, J.W. Lee and W.J. Book, "Dynamic analysis and control of lightweight arms with a parallel mechanism," *Proc. USA-Japan Symp. on Flexible Automation – Crossing Bridges: Adv. Flexible Autom. Rob.*, Minneapolis, Minnesota (1988) pp. 369–374.
16. A. Fattah, J. Angeles and A. K. Misra, "Dynamics of a 3-DOF spatial parallel manipulator with flexible links," *Proc. IEEE International Conference on Robotics and Automation*, Nagoya, Japan (1995) pp. 627–632.
17. D. Sun and J.K. Mills, "PZT actuator placement for structural vibration damping of high speed manufacturing equipment," *Proc. of the American Control Conference, San Diego* (1999) pp. 1107–1111.
18. T. Bailey and J. E. Hubbard Jr., " Distributed piezoelectric-polymer active vibration control of a cantilever beam," *J. Guidance, Control and Dynamics* **8**(5), 605–611 (1985).

https://doi.org/10.1017/S0263574701004039 Published online by Cambridge University Press

APPENDIX

$$M_{11}=(m_s+m)\begin{bmatrix}1&0&0\\0&1&0\\0&0&1\end{bmatrix}\qquad M_{12}=\frac{ml}{2}\begin{bmatrix}s_1&0&0\\0&s_2&0\\0&0&s_3\end{bmatrix}$$

$$M_{14}=m\begin{bmatrix}s_1\int\psi_1\,d\xi&\cdots&s_1\int\psi_r\,d\xi&0&\cdots&0&0&\cdots&0\\0&\cdots&0&s_2\int\psi_1\,d\xi&\cdots&s_2\int\psi_r\,d\xi&0&\cdots&0\\0&\cdots&0&0&\cdots&0&s_3\int\psi_1\,d\xi&\cdots&s_3\int\psi_r\,d\xi\end{bmatrix}$$

$$M_{22}=\frac{ml^2}{3}\begin{bmatrix}1&0&0\\0&1&0\\0&0&1\end{bmatrix}\qquad M_{33}=\begin{bmatrix}m_p&0&0\\0&m_p&0\\0&0&I_P\end{bmatrix}$$

$$M_{24}=ml\begin{bmatrix}\int\psi_1\xi\,d\xi&\cdots&\int\psi_r\xi\,d\xi&0&\cdots&0&0&\cdots&0\\0&\cdots&0&\int\psi_1\xi\,d\xi&\cdots&\int\psi_r\xi\,d\xi&0&\cdots&0\\0&\cdots&0&0&\cdots&0&\int\psi_1\xi\,d\xi&\cdots&\int\psi_r\xi\,d\xi\end{bmatrix}$$

$$M_{44}=ml\begin{bmatrix}\hat{M}&0&0\\0&\hat{M}&0\\0&0&\hat{M}\end{bmatrix}\qquad \hat{M}=\begin{bmatrix}\int\psi_1^2\,d\xi&\cdots&0\\\vdots&\cdots&\vdots\\0&\cdots&\int\psi_r^2\,d\xi\end{bmatrix}\in R^{r\times r}$$

$$K=\frac{EI}{l^3}\begin{bmatrix}\hat{K}&0&0\\0&\hat{K}&0\\0&0&\hat{K}\end{bmatrix}\qquad \hat{K}=\begin{bmatrix}\int\psi_1''^2\,d\xi&\cdots&0\\\vdots&\cdots&\vdots\\0&\cdots&\int\psi_r''^2\,d\xi\end{bmatrix}\in R^{r\times r}$$

$$V_1=-\begin{bmatrix}0.5mlc_1\dot{\beta}_1^2+\sum_{j=1}^{r}m\dot{\eta}_{1j}\dot{\beta}_1c_1\int\psi_j\,d\xi\\0.5mlc_2\dot{\beta}_2^2+\sum_{j=1}^{r}m\dot{\eta}_{2j}\dot{\beta}_2c_2\int\psi_j\,d\xi\\0.5mlc_1\dot{\beta}_3^2+\sum_{j=1}^{r}m\dot{\eta}_{3j}\dot{\beta}_3c_3\int\psi_j\,d\xi\end{bmatrix}\qquad V_2=m\begin{bmatrix}\sum_{j=1}^{r}\dot{\eta}_{1j}\dot{\rho}_1c_1\int\psi_j\,d\xi\\\sum_{j=1}^{r}\dot{\eta}_{1j}\dot{\rho}_1c_1\int\psi_j\,d\xi\\\sum_{j=1}^{r}\dot{\eta}_{1j}\dot{\rho}_1c_1\int\psi_j\,d\xi\end{bmatrix}$$

https://doi.org/10.1017/S0263574701004039 Published online by Cambridge University Press

$$V_4 = -m \begin{bmatrix} c_1 \dot{\rho}_1 \dot{\beta}_1 \int \psi_1 \, d\xi \\ \vdots \\ c_1 \dot{\rho}_1 \dot{\beta}_1 \int \psi_r \, d\xi \\ c_2 \dot{\rho}_2 \dot{\beta}_2 \int \psi_1 \, d\xi \\ \vdots \\ c_2 \dot{\rho}_2 \dot{\beta}_2 \int \psi_r \, d\xi \\ c_3 \dot{\rho}_3 \dot{\beta}_3 \int \psi_1 \, d\xi \\ \vdots \\ c_3 \dot{\rho}_3 \dot{\beta}_3 \int \psi_r \, d\xi \end{bmatrix} \in R^{3r}$$

where $s_i = \sin(\alpha_i - \beta_i)$ and $c_i = \cos(\alpha_i - \beta_i)$

$$F = [F_1 \quad F_2 \quad F_3]^T$$

$$J_{\Gamma 1} = \begin{bmatrix} \cos\alpha_1 & \sin\alpha_1 & 0 & 0 & 0 & 0 \\ 0 & 0 & \cos\alpha_2 & \sin\alpha_2 & 0 & 0 \\ 0 & 0 & 0 & 0 & \cos\alpha_3 & \sin\alpha_3 \end{bmatrix}$$

$$J_{\Gamma 2} = \begin{bmatrix} s2_1 & c2_1 & 0 & 0 & 0 & 0 & 0 \\ 0 & 0 & s2_2 & s2_2 & c2_2 & 0 & 0 \\ 0 & 0 & 0 & 0 & 0 & s2_3 & c2_3 \end{bmatrix}$$

where $s2_i = -l \sin\beta_i - \cos\beta_i \sum_{j=1}^{r} \eta_{ij}$ and $c2_i = l \cos\beta_i - \sin\beta_i \sum_{j=1}^{r} \eta_{ij}$

$$J_{\Gamma 3} = \begin{bmatrix} -1 & 0 & -1 & 0 & -1 & 0 \\ 0 & -1 & 0 & -1 & 0 & -1 \\ s3_1 & -c3_1 & s3_2 & -c3_2 & s3_3 & -c3_3 \end{bmatrix}$$

where $s3_i = r \sin(\varphi_i + \varphi)$ $c3_i = r \cos(\varphi_i + \varphi)$

$$J_{\Gamma 4} = \begin{bmatrix} -\sin\beta_1 & \cos\beta_1 & & & & \\ \vdots & \vdots & 0 & & 0 & \\ -\sin\beta_1 & \cos\beta_1 & & & & \\ & & -\sin\beta_2 & \cos\beta_2 & & \\ 0 & & \vdots & \vdots & 0 & \\ & & -\sin\beta_2 & \cos\beta_2 & & \\ & & & & -\sin\beta_3 & \cos\beta_3 \\ 0 & & 0 & & \vdots & \vdots \\ & & & & -\sin\beta_3 & \cos\beta_3 \end{bmatrix} \in R^{3r \times 6}$$

https://doi.org/10.1017/S0263574701004039 Published online by Cambridge University Press